Journal of Materials Chemistry C

Accepted Manuscript

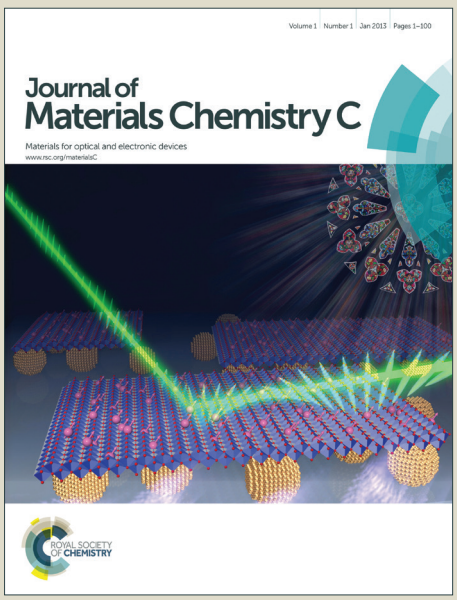

ROYAL SOCIETY OF CHEMISTRY

www.rsc.org/materialsC

Optical properties of Nd^{3+} and Yb^{3+} -doped $AgM(IO_3)_4$ metal iodates: transparent host matrices for mid-IR lasers and nonlinear materials.

Delphine Phanon [I], Yan Suffren [I], Mohamed B. Taouti [II], Djamal Benbertal [II], Alain Brenier [III], Isabelle Gautier-Luneau [I*]

[I] Université Grenoble Alpes, Institut NEEL, F-38042 Grenoble, France

[II] Université de Laghouat, Laboratoire de Physico-Chimie des Matériaux, BP 37G. Laghouat 03000, Algérie

[III] Institut Lumière Matière, UMR5306 Université Lyon 1-CNRS, Université de Lyon, 69622 Villeurbanne cedex, France

[*]Corresponding author: Isabelle.Gautier-Luneau@neel.cnrs.fr

Fax: +33 4 76 88 10 38; Tel: + 33 4 76 88 78 04

Keywords: crystal engineering / iodine / IR spectroscopy / nonlinear optics / Rare earth

Summary

Nine new isomorphic iodate compounds Na$M$$(IO_3)_4$ with M = Y, Nd, Gd and AgM'$(IO_3)_4$ with M' = Y, La, Nd, Eu, Gd, Bi have been synthesized either by evaporation of concentrated nitric acid solution or by hydrothermal synthesis. They crystallize in the monoclinic acentric *Cc* space group. Typical unit cell parameters for $AgY(IO_3)_4$ are a = 31.277(3) Å, b = 5.547(1) Å, c = 12.556(2) Å, β = 91.11(2)°, V = 2178.0(6) Å^3 and Z = 8. Crystal structures have been solved on single crystals for $NaY(IO_3)_4$, $AgY(IO_3)_4$, $AgLa(IO_3)_4$, $AgGd(IO_3)_4$ and $AgBi(IO_3)_4$ and on powder for $NaNd(IO_3)_4$, $NaGd(IO_3)_4$, $AgEu(IO_3)_4$ and $AgGd(IO_3)_4$. They are thermally stable up to 550°C for $NaY(IO_3)_4$, 430°C for $AgY(IO_3)_4$, 500°C for $AgLa(IO_3)_4$ and 490°C for $AgBi(IO_3)_4$. The crystal structure reveals two-dimensional layered network. The sheets are connected together by I···O interactions. All these metal iodates generate second harmonics and are transparent up to 12 μm. So they are interesting as potential laser matrices in the mid and beginning of the far-infrared. The properties of Nd^{3+} and Yb^{3+} -doped $AgGd(IO_3)_4$ and of Nd^{3+} -doped $AgLa(IO_3)_4$ have been studied.

Introduction

Since the 70's years, metal iodates have been extensively studied by several teams such as Bell Laboratories for their nonlinear optical (NLO) properties but also for ferroelectric, piezoelectric and pyroelectric properties,[1-8] The interest for these compounds has resumed in the early 2000's,[9-21] also for the ionic conductivity of α-$LiIO_3$,[22-23] and for the radiation stability of actinide iodates.[24-26] We have shown that metal iodates are particularly interesting for infrared applications, as they possess a large domain of transparency from visible to the beginning of the far IR (12.5 μm), thus covering the three atmospheric transparency windows.[27-29] For mid and far IR NLO crystals, the challenge is important, and

especially in the third atmospheric transparency windows (band III: 8 – 12 μm).[30-31] Chalcopyrites such as $AgGaX_2$ (X = S, Se) and $ZnGeP_2$ or halides like $CsGeBr_3$ and Tl_4HgI_6, are transparent in this spectral range but are limited in their applications.[32-33] $ZnGeP_2$ or $AgGaSe_2$ are the main commercialized materials.

In addition, another interest is to obtain bifunctional materials: self-doubling crystals based on a nonlinear matrix doped with lanthanide fluorescent ions.[34-35] Luminescence properties of Cr^{3+} -doped α-$In(IO_3)_3$[29] and Nd^{3+}, Yb^{3+} -doped $Y(IO_3)_3$ have already been observed.[36] The laser emission should be in the visible or in the infrared range as most of iodate hosts are transparent in these domains.

In this paper, we present the study of acentric bimetallic iodates which are all together isotructural: $NaM(IO_3)_4$ (with M = Y, Nd, Gd) and $AgM'(IO_3)_4$ (with M' = Y, La, Nd, Eu, Gd, Bi). Crystal structure of $NaY(IO_3)_4$, $AgY(IO_3)_4$, $AgLa(IO_3)_4$, $AgGd(IO_3)_4$, and $AgBi(IO_3)_4$ have been realized. For $NaNd(IO_3)_4$, $NaGd(IO_3)_4$, $AgEu(IO_3)_4$ and $AgGd(IO_3)_4$ compounds, no single crystal was available, thus the structure refinements have been carried out by X-ray powder diffraction. Thermal analyses, SHG tests and powder optical damage thresholds have been performed and IR spectroscopy enables the determination of the domain of transparency. As these compounds are isostructural, all combinations of lanthanides can be inserted in order to vary the luminescence properties of as-prepared materials. The present work reports on the characterisation of Nd^{3+} and Yb^{3+} -doped $AgGd(IO_3)_4$ and Nd^{3+} -doped $AgLa(IO_3)_4$ *via* spectroscopic studies.

Results and discussion

1. Crystal structure description

The crystal structure description will be based on the $AgY(IO_3)_4$ compound, as all of the compounds are isostructural. Selected interatomic distances are presented in Table 1 for

$AgY(IO_3)_4$. In Table 2 are reported limit interatomic distances and limit bond angles for all studied compounds.

$AgY(IO_3)_4$ compound crystallizes in the monoclinic system, *Cc* space group. The asymmetric unit is made up of two yttrium atoms, two silver atoms and eight iodate groups. All metal ions in the structure are surrounded by eight oxygen atoms. For both yttrium atoms, oxygen atoms are provided by eight iodate groups: 2 $I(1)O_3$, 1 $I(2)O_3$, 3 $I(3)O_3$ and 2 $I(4)O_3$ for Y1 and 1 $I(4)O_3$, 1 $I(5)O_3$, 2 $I(6)O_3$, 1 $I(7)O_3$ and 3 $I(8)O_3$ for Y2, respectively. The Y1 atom is in a distorted square antiprismatic environment. The mean deviations from a calculated plane of the two square faces are equal to 0.229 Å and 0.022 Å respectively. The dihedral angle between these two faces is equal to 10.2°. The Y1-O bond lengths are in the range 2.279(6) Å to 2.423(6) Å. The coordination polyhedron of the Y2 yttrium atom is a bicapped trigonal prism with a dihedral angle between the trigonal faces equal to 5.5°. The two capped atoms are distant from the Y2 atom of 2.286(6) Å and 2.502(6) Å which correspond to the shorter and to the longer Y2-O bond lengths respectively.

For silver atoms, the eight oxygen atoms are provided by six iodate groups for Ag1: 2 $I(4)O_3$, 3 $I(5)O_3$ 1 $I(8)O_3$), and by five iodate groups for Ag2 (1 $I(1)O_3$, 2 $I(3)O_3$, 1 $I(4)O_3$ and 1 $I(5)O_3$, respectively. Two and three iodate groups are chelating for Ag1 and Ag2, respectively. For both Ag ions, the coordination polyhedron is a distorted cube in which seven oxygen atoms well describe the tops of the cube and the eighth is outside this cube due to a constrained environment of a chelate iodate group. The cube environment of Ag2 is less distorted than the one observed for Ag1. The Ag-O bond lengths are in the range 2.344(7) Å - 3.070(6) Å and 2.379(6) Å - 2.875(6) Å for Ag1 and Ag2, respectively. Bond-valence sum calculations resulted in values of 0.95 and 0.96 for Ag^+, 3.02 and 3.08 for Y^{3+}.[37]

The iodine atoms of iodate anions have the usual tetrahedral arrangement (with I-O bond lengths in the range 1.787(6) Å to 1.835(6) Å) completed by three I···O interactions (in the range 2.449(6) Å to 3.057(6) Å) arranged around the lone pair direction leading to an octahedral geometry.[38] In a the previous description of $NaYI_4O_{12}$, a different choice of lengths for the I-O bonds led to IO_4 groups designed with three I-O bond lengths comprised in the range 1.79(2) to 1.82(2) Å and a fourth one above 2.42(2) Å.[39] We have shown that this latter is better described as I···O interaction.[40] Bond-valence sum calculations of I^{5+} iodine ions are in the range 5.31 to 5.5.[37] The difference between calculated and theorical BVS values for iodine atoms is due to the coordination polyhedron distortion influenced by the presence of lone electron pair.[41] The eight iodate groups show six different coordination schemes towards cations linking one to six metallic atoms through μ_2-O or μ_3-O bridging oxygen atoms (see the Supporting Information). In a similar dense structure (α-AgIO3), one oxygen atom of each iodate group is μ_4-O bridging.[42]

The crystal structure of $AgY(IO_3)_4$ consists of sheets parallel to the (100) plane (Fig. 1) The sheet thickness is equal to *a/2* (15.638 Å). The cohesion of crystal packing is assumed by six kinds of I···O interactions between the sheets, with distances in the range 2.542(6) Å to 3.057(6) Å. Oxygen atoms involved in these interactions are not coordinated to cations. In a sheet, the $\{MO_8\}$ polyhedral (with *M* = Ag or Y) are connected by edge-sharing through μ_2-O and μ_3-O atoms of iodate groups leading to shorter *M*···*M* distances comprised between 3.678(1) and 4.274(1) Å. So, each $\{Ag(1)O_8\}$ polyhedron is linked by edge-sharing to five metals: two Ag2, two Y2 and one Y1 atoms. The $\{Ag(2)O_8\}$ polyhedron is bonded to three Y1 atoms, in addition of the two Ag1 atoms. The $\{YO_8\}$ polyhedra are only linked to silver atoms, mentioned above. Moreover, the polyhedra are connected via (*M*-O-I-O-*M*) bridging iodate groups leading to M···M longer distances in the range 5.547(1) to 5.737(7) Å.

DSC analyses show the compounds are thermally stable up to 550°C for $NaY(IO_3)_4$, 430°C for $AgY(IO_3)_4$, 500°C for $AgLa(IO_3)_4$ and 490°C for $AgBi(IO_3)_4$.

2. Second Harmonic Generation (SHG) and powder optical damage threshold

Kurtz and Perry powder tests have been done leading to a qualitative estimation of the intensity of the SHG signal.[43] The intensities of SHG light generated by the $NaM(IO_3)_4$ (with M = Y, Gd) and $AgM'(IO_3)_4$ (with M' = Y, Gd, Bi) iodates compounds have been compared and results are the following: $NaGd(IO_3)_4$ ~ $AgGd(IO_3)_4$ < $AgBi(IO_3)_4$ <$AgLa(IO_3)_4$ < $AgY(IO_3)_4$ < $NaY(IO_3)_4$ < α-$LiIO_3$. This comparison allows us to give a maximal estimation of nonlinear coefficients d_{ij} of several pm.V^{-1} for these iodates as measured for α-$LiIO_3$ (d_{31}= 7.11, d_{33} = 7.02 pm.V^{-1} for α-$LiIO_3$).[44] However these latters compared to the values obtained by converse piezoelectric measurements are one order of magnitude lower. Indeed, the d_{33} piezoelectric charge constant was estimated to 92 pm.V^{-1} and 138 pm.V^{-1} for $LiIO_3$ and $NaYI_4O_{12}$, respectively.[39] Consequently, only crystals with millimetric sizes will enable the measurement of the phase-matching properties of sum- and difference- frequency generations as well as the dispersion equations of the refractive indice and of the nonlinear coefficients of these compounds over their transparency range.[45-47]

The present compounds show high optical damage thresholds on powders. Compare to the α-$LiIO_3$ one, they are equivalents: $AgGd(IO_3)_4$, 2.5 ± 0.3 GW.cm^{-2}; α-$LiIO_3$, 3.0 ± 0.3 GW.cm^{-2}; $NaGd(IO_3)_4$, 3.6 ± 0.3 GW.cm^{-2}; $NaY(IO_3)_4$, $AgY(IO_3)_4$, $AgBi(IO_3)_4$, 4.2 ± 0.3 GW.cm^{-2} (for Nd^{3+}:YAG laser operating at 1.064 μm and generating pulses of 150 ps duration every 200 ms). They have been determined on powders, so the values measured on single crystals will be higher; for example α-$LiIO_3$, which is the reference compound, has an optical damage threshold on single crystal equal to 8 GW.cm^{-2}.[44] These values are closed to the ones measured at the same wavelength on commercial single crystals: 23 GW.cm^{-2} for KDP with

pulses of 200 ps and 10 GW.cm^{-2} for BBO with pulses of 100 ps.[44] These iodates are thus very interesting because of both their good optical damage thresholds and high nonlinear coefficients.

3. Transparency range

Optical reflectance data in the 2.5 to 16 μm range is given for $NaY(IO_3)_4$, $NaGd(IO_3)_4$, $AgY(IO_3)_4$, $AgLa(IO_3)_4$, $AgGd(IO_3)_4$ and $AgBi(IO_3)_4$ compounds in Fig. 2. Transmittance curves of compounds are rather similar. There is no absorption band up to 12 μm. The absence in these IR spectra of any H_2O absorption band underlines their non hygroscopicity. Absorption bands observed beyond 12 μm are due to vibrations corresponding to the IO_3^- group. The free IO_3^- ion has a pyramidal structure and is assigned to the C_{3v} symmetry point group. According to the selection rules, the IO_3^- IR spectrum is characterised (in aqueous solution) by four fundamental vibrations: *A* symmetric stretching mode (υ_1 = 805 cm^{-1} (12.4 μm)), *E* antisymmetric stretching mode (υ_3 = 775 cm^{-1} (12.9 μm)), *A* symmetric deformation mode (υ_2 = 358 cm^{-1} (27.9 μm)) and *E* antisymmetric deformation mode (υ_4 = 320 cm^{-1} (31.3 μm)).[48] Thus the dominant absorption band found between 12 and 15 μm in compounds can be expected to contain υ_1, $2\upsilon_2$, υ_{3a}, υ_{3b}, $2\upsilon_4$ et $\upsilon_2+\upsilon_4$.[49] This work gives evidence that the bimetallic iodates studied, are transparent in both atmospheric transparency windows (bands II and III). They present a spectroscopic behaviour similar to $M(IO_3)_2$ (*M* = Hg, Zn, Mn, Mg, Ni, Co),[11, 27] $M(IO_3)_3$ (*M* = Fe, Ga, In)[29] and $Y(IO_3)_3$.[28]

4. Nd^{3+} -doped anhydrous gadolinium silver iodate and lanthanum silver iodate

The room temperature emission spectra of $AgGd(IO_3)_4:Nd^{3+}$ obtained upon photoexcitation of the $^4F_{3/2}$ excited multiplet state of the neodymium ion at 750 nm (Fig. 3), show emission lines originating from $^4F_{3/2} \rightarrow {}^4I_{11/2}$ transition centred at approximately 1060

nm. The $^4F_{3/2}$ and $^4I_{11/2}$ excited multiplet states split into two and six levels respectively and the number of the observed Stark components in these compounds is equal to 7.

The fluorescence decay times in $AgGd_{1-x}Nd_x(IO_3)_4$ and $AgLa_{1-x}Nd_x(IO_3)_4$ have been measured for several Nd^{3+}concentrations. The decays of all these emissions are exponential and can be fitted by an exponential function $y = Ae^{-x/t_0}$ with t_0 corresponding to the Nd^{3+} fluorescence lifetime. Values of t_o are displayed in Table 3. A non-radiative energy transfer occurs and increases with Nd^{3+} concentration, that's why the Nd^{3+} fluorescence lifetime decreases (Fig. 4). The useful Nd^{3+} concentration for laser applications[50] is estimated to be equal or less than 2 at% for these hosts. The fluorescence of both hosts is similar whatever the Nd^{3+} concentrations. A comparison with the fluorescence of two others iodate compounds α-$Y(IO_3)_3$ and β-$Y(IO_3)_3$ already studied, shows that until 5 at.% of Nd^{3+} β-$Y(IO_3)_3$ is a best host.[36] Whereas the α-$Y(IO_3)_3$ host has higher fluorescence lifetime over all Nd^{3+} concentrations studied than $AgGd(IO_3)_4$ and $AgLa(IO_3)_4$ hosts.

5. Yb^{3+} -doped anhydrous gadolinium silver iodate

In comparison with the neodymium ion, the ytterbium ion has several advantages due to its very simple energy scheme, only two energy levels ($^2F_{5/2} \rightarrow {}^2F_{7/2}$ transition): no excited state absorption and it is possible to avoid concentration quenching within a large domain. Furthermore, the small quantum defect contributes to weak thermal effects so that Yb^{3+} -doped materials are interesting for efficient high-power continuous-wave lasers. Another advantage of Yb^{3+} -doped materials is to bring new advances in diode-pumped ultra-short sources in the femtosecond scale of time by playing with the Yb^{3+} wide-fluorescence spectrum (superposition of several emissions with close energy). The $^2F_{5/2}$ excited multiplet state splits into three Stark levels and the $^2F_{7/2}$ multiplet ground state splits in four levels.

The room temperature emission spectra of $AgGd(IO_3)_4:Yb^{3+}$ obtained upon photoexcitation of the $^2F_{5/2}$ excited multiplet state at 980 nm (Fig. 5) show a narrow emission line at approximately 980 nm and another very broad band (width equal to 35 nm, between 985 and 1020 nm), due to the $^2F_{5/2} \rightarrow {}^2F_{7/2}$ transition. The 980 nm wavelength corresponds to both emission and absorption, so it is hardly usable for laser emission. Precise assignments of the observed bands are not possible at room temperature and only measurements at low temperature allow it.

As for the Nd^{3+} ions, the fluorescence decay times in $AgGd_{1-x}Yb_x(IO_3)_4$ have been measured for several Yb^{3+}concentrations. Values of t_o are displayed in Table 3. The fluorescence lifetime decreases continuously from 2 to 17 at% due to energy migration and trapping effects. These effects are in competition with the $^2F_{7/2} \rightarrow {}^2F_{5/2}$ radiative reabsorption which increases the measured lifetime[50] and leads very often to a lifetime maximum such as the casesof α-$Y(IO_3)_3$ and β-$Y(IO_3)_3$ (Fig. 6).[36] The optimal concentration of Yb^{3+} for laser applications is a difficult task (it is a quasi-three level laser) but it is likely to belong in the range in the present study.

Considering the metal atoms only connected *via* iodate bridges, four Gd···Gd distances (b=5.581 Å) in $AgGd(IO_3)_4$ compounds are observed. They are shorter than those observed in α-$Y(IO_3)_3$ (seven Y···Y mean distances at 6.399 Å) and β-$Y(IO_3)_3$ (six mean distance at 5.701 Å) compounds. This difference could explain the shorter fluorescence lifetimes of Nd^{3+} and Yb^{3+} ions in $AgGd_{1-x}Yb_x(IO_3)_4$ compounds.

Conclusion

The $NaM(IO_3)_4$ with M = Y, Nd, Gd and $AgM'(IO_3)_4$ with M' = Y, La, Nd, Eu, Gd, Bi compounds are isostructural and crystallize in the monoclinic acentric *Cc* space group. These nonlinear optical compounds exhibit good optical damage thresholds, broad windows of transparency (up to 12 μm) and good thermal stabilities and are not hygroscopic. The metal

(III) atoms having similar ionic radii and same coordination spheres, all lanthanide combinations can be inserted in order to vary the luminescence properties of as-prepared materials. Luminescence phenomena have been observed in $AgGd(IO_3)_4:Nd^{3+}$ and $-Yb^{3+}$ and in $AgLa(IO_3)_4:Nd^{3+}$. Nd^{3+} and Yb^{3+} concentrations dependence of the decay times have been measured and allow us to determine the useful concentration of lanthanide ions for laser applications: about 2 at% for Nd^{3+} and Yb^{3+}. At the present time, few laser emissions have been pointed out in the mid-infrared (5-10 μm). Only one Er^{3+} laser emission was observed in oxide host at around 5 μm.[51] However, no host was transparent beyond 6 μm so no laser emission was detected beyond this value. These new compounds being transparent until 12 μm, it should be possible to observed laser emissions in the mid-infrared and in the beginning of the far-infrared.

Experimental

Materials: All reagents and chemicals were purchased from commercial sources and used without further purification.

Syntheses of $NaM(IO_3)_4$, (M = Y, Nd, Gd) compounds have been obtained under hydrothermal conditions. The metal nitrates (yttrium, neodymium or gadolinium) and sodium iodate, with a Na/M ratio equal to 10 for Y, Nd compounds and 15 for Gd compound respectively, are dissolved in 10 mL of aqueous solution. The resulting solutions are put into a Teflon steel autoclave. After sealed, the autoclave is heated to 200°C in furnace and held at this temperature during 24 h for Y and Nd compounds and during 60 h for Gd compound. Then the autoclave is gradually cooled at 20°C/h until 40°C. Crystals obtained in a colourless solution, are filtered, washed with deionised water and dried in oven. Colourless platelets suitable for XRD on single crystal are obtained for $NaY(IO_3)_4$. Tiny colourless platelets and tiny violet needles are obtained for $NaGd(IO_3)_4$ and $NaNd(IO_3)_4$, respectively. The mean

yields are 95 mol%, 87 mol% and 70 mol% for Y, Nd, and Gd compounds respectively. Elemental analysis (Found: Na, 2.74; Gd, 17.39; I 57.26. $NaGdI_4O_{12}$ requires Na, 2.61; Gd, 17.87; I, 57.69%).

Syntheses of Ag*M*$(IO_3)_4$, (*M* = Y, La, Nd, Eu, Gd) compounds are obtained under hydrothermal conditions. Metal nitrates in equi-molar ratio are dissolved with four equivalents of iodic acid in 10 mL aqueous solution. The resulting solutions are put into a Teflon-lined steel autoclave. After sealed, the autoclave is heated to 200°C in furnace and held at this temperature, 24 h for Y, Nd and Eu compounds, 48 h for La compound and 60 h for Gd compound. Then the autoclave is gradually cooled at 15°C/h until room temperature before open it. Crystals, obtained in a colourless solution are filtered, washed with deionised water and dried in oven. Colourless platelets suitable crystals for XRD on single crystal are only obtained for Y, La and Gd compounds. Tiny colourless crystals and tiny violet crystals are obtained for $AgEu(IO_3)_4$ and $AgNd(IO_3)_4$. The mean yields are 98 mol% for La, 93 mol% for Nd and Gd and 90 mol% for Y and Eu compounds. Iodine concentration is not titrated in the presence of silver. Elemental analyses (Found: Ag, 12.58; Y, 9.70. $AgYI_4O_{12}$ requires Ag, 12.03; Y, 9.92; I, 56.63%; Found: Ag, 10.91; Gd, 15.86. $AgGdI_4O_{12}$ requires Ag, 11.18; Gd, 16.30; I, 52.62%; Found: Ag, 11.58; La, 15.56. $AgLaI_4O_{12}$ requires Ag, 11.40; La, 14.68; I, 53.64%).

The Nd^{3+} and Yb^{3+} -doped $AgGd(IO_3)_4$ and Nd^{3+} -doped $AgLa(IO_3)_4$ were synthesized in the same manner as the pure phases with the following molar ratio $([M^{3+}]+[Ln^{3+}])/[IO_3^-] = 1/4$ and $[Ag^+]/[IO_3^-] = 1/4$. The composition of each phase was determined by elementary analyses and corresponds exactly to the expected nominal value.

Synthesis of $AgBi(IO_3)_4$: Under hydrothermal conditions, a mixture of $AgIO_3$ and $AgBi(IO_3)_4$ is obtained. An $AgBi(IO_3)_4$ pure phase is obtained in the following conditions: 10^{-3} moles of bismuth nitrate, 10^{-3} moles of silver nitrate and 4.10^{-3} moles of iodic acid are

dissolved in 100 mL of nitric acid solution (7M). The solution is heated at 100°C during 24h. By slow evaporation of the solution, colourless platelets suitable for XRD on single crystal are obtained. They are filtered, washed with deionised water and dried in oven. Mean yield is 90 mol%. Elemental analysis (Found: Ag, 10.59; Bi, 20.03. $AgBiI_4O_{12}$ requires Ag, 10.61; Bi, 20.56; I, 49.94%).

Crystal structure determination: Crystal data of $NaY(IO_3)_4$, $AgY(IO_3)_4$, $AgLa(IO_3)_4$, $AgGd(IO_3)_4$ and $AgBi(IO_3)_4$ together with details of diffraction experiment and refinement, are summarised in Table 4. Crystals were mounted on a Nonius four circle diffractometer equipped with a CCD two-dimensional detector, using monochromatic silver radiation (λ = 0.56087 Å) at 293 K. The reflections were corrected for Lorentz and polarization effects. An absorption correction was applied using the empirical method SADABS.[52] All structures were solved by direct methods with SIR92 program[53] and refined by full matrix least-squares, based on F^2, using the Shelxl software[52] through the WinGX program suite.[54] Final refinement was performed with anisotropic thermal parameters for all atoms, taking into account the contribution of the inverted component of a racemic twin.

Further details of the crystal structure investigations may be obtained from the Fachinformationszentrum Karlsruhe, 76344 Eggenstein-Leopoldshafen, Germany, on quoting the depository numbers CSD-427148 – CSD-427152.

Structure refinements on powder: X-ray powder diffraction patterns were recorded on a D8 Bruker Advance diffractometer (Cu $K_{\alpha 1}$ radiation, λ = 1.54056 Å) in $\theta/2\theta$ configuration equipped with a Ge (111) monochromator. They were collected under air between 16° and 90° in 2θ with a step of 0.014° or between 10° and 100° with a step of 0.009°. The samples were carefully ground prior to the measurements. The $NaNd(IO_3)_4$, $NaGd(IO_3)_4$, $AgNd(IO_3)_4$ and $AgEu(IO_3)_4$ compounds are isostructural with $NaY(IO_3)_4$, $AgY(IO_3)_4$, $AgLa(IO_3)_4$, $AgGd(IO_3)_4$ and $AgBi(IO_3)_4$. So, their structures were refined by using the obtained structural

model of $AgY(IO_3)_4$. The structure refinements were carried out with the Rietveld method using the Fullprof program.[55] First of all, atomic coordinates of all atoms except oxygen atoms were refined. Then, each iodate group was refined separately; iodine atom was fixed and positions of oxygen atoms were refined by using constraints on distances and angles. Final refinement was carried out by refining all atoms. Preferential orientation has been observed along the [010] direction for $NaNd(IO_3)_4$ and $AgNd(IO_3)_4$ compounds and along the [100] direction for $NaGd(IO_3)_4$.

Details of the data collection and Rietveld refinements are summarized in Table 5 and the final Rietveld profile is shown in Fig. 7 only for the $AgEu(IO_3)_4$ compound. Other patterns are in the Supporting Information. For $NaNd(IO_3)_4$, the factor of reliability R_{wp} is large (26.9%) because of background. The chosen step size was too small (0.009°) and statistic is not fine.

Second harmonic generation: Kurtz and Perry powder tests have been done leading to a qualitative estimation of the intensity of the SHG signal,[43] using the fundamental beam emitted by a Q-switched, mode-locked Nd^{3+}:YAG laser operating at 1.064 μm and generating pulses of 150 ps duration every 200 ms. So, the NLO efficiency was estimated by visual comparison (see Fig.S9). For all samples, the same quantity of product has been ground and sieved in the same manner in order to make comparison and placed between two glass sheets then put in front of an infrared beam (λ = 1.064 μm). In order to determine the optical damage thresholds, energy of the laser emission is gradually increased until samples become brown.

IR spectroscopy: Optical absorption spectra were run on a Nicolet Magna 550 spectrometer in the 4 000 to 625 cm^{-1} region (2.5 to 16 μm), using the ATR technique with a diamond crystal. The transmittance has been measured on a wide range spanning the near-IR to the far-IR on polycrystalline materials of $NaY(IO_3)_4$ and $AgM(IO_3)_4$ with *M* = Y, La, Nd, Eu, Gd and Bi. Before recordings, these compounds were kept at room temperature without any particular caution.

Spectral and fluorescence lifetime measurement: Fluorescence spectra and their decays under pulsed laser excitation in the $^4F_{3/2}$ and $^2F_{7/2}$ multiplets of the Nd^{3+} and Yb^{3+} ground configuration respectively were excited using a tunable dye laser from Laser Analytical Systems pumped with a frequency-doubled Nd:YAG laser from BM Industries delivering pulses of 10 ns duration with a 10 Hz repetition rate. The visible radiation from the dye laser was around 750 or 805 nm for Nd^{3+}. For Yb^{3+} it was around 696 nm and then it was converted in the near infrared range near 980 nm with a hydrogen cell Raman shifter. The luminescence was detected by a Hamamatsu R1767 photomultiplier through a Jobin Yvon monochromator equipped with a 1 μm blazed grating. The resulting signal was then processed using a SR250 gated integrator and boxcar averager from Stanford Research Systems, providing a signal to a DAC card inserted in a computer. The time evolutions of the fluorescences were recorded with a Lecroy 9410 digital oscilloscope coupled to the same computer.

Supplementary information: X-ray powder diffraction patterns of $NaNd(IO_3)_4$, $NaGd(IO_3)_4$ and $AgNd(IO_3)_4$ measured on D8 Bruker (λ = 1.54056 Å). Coordination schemes of iodate anion towards cations in $NaM(IO_3)_4$, M = Y, Nd, Gd and $AgM'(IO_3)_4$, M'= Y, La, Nd, Eu, Gd, Bi. Coordination sphere details of metals in $AgY(IO_3)_4$, showing the nearest metal neighbors. DSC analyses.

Acknowledgements

We thank Dr. Corinne Felix for his technical assistance concerning the SHG analyses.

References

1 A. Rosenzweig, B. Morosin, *Acta Cryst.*, 1966, **20**, 758-761.
2 S. C. Abrahams, R. C. Sherwood, J. L. Bernstein, K. Nassau, *J. Solid State Chem.*, 1973, **7**, 205-212.
3 K. Nassau, J. W. Shiever, B. E. Prescott, *J. Solid State Chem.*, 1973, **7**, 186-204.
4 S. C. Abrahams, J. L. Bernstein, K. Nassau, *J. Solid State Chem.*, 1976, **16**, 173-184.
5 M. Jansen, *J. Solid State Chem.*, 1976, **17**, 1-6.
6 R. Liminga, S. C. Abrahams, J. L. Bernstein, *J. Chem. Phys.*, 1977, **67**, 1015-1023.
7 S. C. Abrahams, J. L. Bernstein, *Solid State Commun.*, 1978, **27**, 973-976.
8 C. Svensson, S. C. Abrahams, J. L. Bernstein, *J. Solid State Chem.*, 1981, **36**, 195-204.
9 P. S. Halasyamani, K. R. Poeppelmeier, *Chem. Mater.*, 1998, **10**, 2753-2769.
10 R. E. Sykora, K. M. Ok, P. S. Halasyamani, D. M. Wells, T. E. Albrecht-Schmitt, *Chem. Mater.*, 2002, **14**, 2741-2749.
11 B. Bentria, D. Benbertal, M. Bagieu-Beucher, A. Mosset, J. Zaccaro, *Solid State Sci.*, 2003, **5**, 359-365.
12 M. Weil, *Z. Naturforsch., B: Chem. Sci.*, 2003, **58**, 627-632.
13 X. A. Chen, H. P. Xue, X. A. Chang, L. Zhang, H. G. Zang, W. Q. Xiao, *J. Alloys Compd.*, 2006, **415**, 261-265.
14 N. Ngo, K. Kalachnikova, Z. Assefa, R. G. Haire, R. E. Sykora, *J. Solid State Chem.*, 2006, **179**, 3824-3830.
15 D. Phanon, B. Bentria, E. Jeanneau, D. Benbertal, A. Mosset, I. Gautier-Luneau, *Z. Kristallogr.*, 2006, **221**, 635-642.
16 X. A. Chen, L. Zhang, X. N. Chang, H. P. Xue, H. G. Zang, W. Q. Xiao, X. M. Song, H. Yan, *J. Alloys Compd.*, 2007, **428**, 54-58.
17 D. Phanon, I. Gautier-Luneau, *Angew. Chem. Int. Ed.*, 2007, **46**, 8488-8491.
18 H. Y. Chang, S. H. Kim, P. S. Halasyamani, K. M. Ok, *J. Am. Chem. Soc.*, 2009, **131**, 2426-2427.
19 S. M. Ravi Kumar, N. Melikechi, S. Selvakumar, P. Sagayaraj, *J. Cryst. Growth*, 2009, **311**, 337-341.
20 C. F. Sun, C. L. Hu, X. Xu, J. B. Ling, T. Hu, F. Kong, X. F. Long, J. G. Mao, *J. Am. Chem. Soc.*, 2009, **131**, 9486-9487.
21 Y. Suffren, I. Gautier-Luneau, *Eur. J. Inorg. Chem.*, 2012, 4264-4267.
22 Y. Mugnier, C. Galez, J. M. Crettez, P. Bourson, J. Bouillot, *Ferroelectrics*, 2001, **257**, 141-146.
23 Y. Mugnier, C. Galez, J. M. Crettez, P. Bourson, C. Opagiste, J. Bouillot, *J. Solid State Chem.*, 2002, **168**, 76-84.
24 A. C. Bean, T. E. Albrecht-Schmitt, *J. Solid State Chem.*, 2001, **161**, 416-423.
25 A. C. Bean, M. Ruf, T. E. Albrecht-Schmitt, *Inorg. Chem.*, 2001, **40**, 3959-3963.
26 R. E. Sykora, K. M. Ok, P. S. Halasyamani, T. E. Albrecht-Schmitt, *J. Am. Chem. Soc.*, 2002, **124**, 1951-1957.
27 D. Phanon, B. Bentria, D. Benbertal, A. Mosset, I. Gautier-Luneau, *Solid State Sci.*, 2006, **8**, 1466-1472.
28 D. Phanon, A. Mosset, I. Gautier-Luneau, *Solid State Sci.*, 2007, **9**, 496-505.
29 D. Phanon, A. Mosset, I. Gautier-Luneau, *J. Mater. Chem.*, 2007, **17**, 1123-1130.
30 G. Boyd, E. Buehler, F. Storz, J. Wernick, *IEEE J. Quantum Electron.*, 1972, **8**, 419-426.
31 W. Chen, G. Mouret, D. Boucher, F. K. Tittel, *Appl. Phys. B-Lasers Opt.*, 2001, **72**, 873-876.
32 M. C. Ohmer, R. Pandey, B. H. Bairamov, *MRS Bull.*, 1998, **23**, 16-20.

33 N. C. Fernelius, F. K. Hopkins, M. C. Ohmer, *SPIE conf.*, 1999, **3793**, 2-8.
34 A. Brenier, D. Jaque, A. Majchrowski, *Opt. Mater.*, 2006, **28**, 310-323.
35 P. Segonds, S. Joly, B. Boulanger, Y. Petit, C. Félix, B. Ménaert, G. Aka, *J. Opt. Soc. Am.*, 2009, **B26**, 750-753.
36 D. Phanon, A. Brenier, I. Gautier-Luneau, *J. Lum.*, 2009, **129**, 203-207.
37 N. E. Brese, M. O'Keeffe, *Acta Cryst.*, 1991, **B47**, 192-197.
38 I. D. Brown, *J. Solid State Chem.*, 1974, **11**, 214-233.
39 K. M. Ok, P. S. Halasyamani, *Inorg. Chem.*, 2005, **44**, 9353-9359.
40 I. Gautier-Luneau, Y. Suffren, H. Jamet, J. Pilmé, *Z. Anorg. Allg. Chem.*, 2010, **636**, 1368-1379.
41 F. Liebau, X. Wang, *Z. Kristallogr.*, 2005, **220**, 589-591.
42 Y. Suffren, I. Gautier-Luneau, C. Darie, C. Goujon, M. Legendre, O. Leynaud, *Eur. J. Inorg. Chem.*, 2013, 3526-3532.
43 S. A. Kurtz, T. T. Perry, *J. Appl. Phys.*, 1968, **39**, 3798-3813.
44 V. G. Dmitriev, G. G. Gurzadyan, D. N. Nikogosyan, in *Handbook of Nonlinear Optical Crystals*, ed. A. E. Siegman, Springer Series in Optical Sciences, Springer Verlag, 1991, Vol. 64.
45 G. Marnier, B. Boulanger, *Opt. Commun.*, 1989, **72**, 139-143.
46 I. Shoji, T. Kondo, A. Kitamoto, M. Shirane, R. Ito, *J. Opt. Soc. Am. B*, 1997, **14**, 2268-2294.
47 Y. Guillien, B. Ménaert, J. P. Fève, P. Segonds, J. Douady, B. Boulanger, O. Pacaud, *Opt. Mater.*, 2003, **22**, 155-162.
48 D. J. Gardiner, R. B. Girling, R. E. Hester, *J. Mol. Struct.*, 1972, **13**, 105-114.
49 W. E. Dasent, T. C. Waddington, *J. Chem. Soc.*, 1960, 2429-2432.
50 A. Brenier, *J. Opt. Soc. Am. B*, 2006, **23**, 2209-2216.
51 G. Boulon, in *Les solides luminescents inorganiques: un dopage réussi*, Lettre des sciences chimiques du CNRS/L'actualité chimique, novembre 1999, p.96-105.
52 G. M. Sheldrick, SADABS, version 2.10, University of Göttingen, Germany, 2003.
53 A. Altomare, M. Cascarano, C. Giacovazzo, A. Guagliardi, *J. Appl. Cryst.*, 1993, **26**, 343-350.
54 L. J. Farrugia, *J. Appl. Cryst.*, 1999, **32**, 837-838.
55 T. Roisnel, J. Rodriguez-Carvajal, in *Materials Science Forum, Proceedings of the Seventh European Powder Diffraction Conference (EPDIC 7)* (Eds.: R. Delhez, E. J. Mittenmeijer), **2000**, pp. 118-123.

Table 1 Selected interatomic distances (Å) (with e.s.d) in $AgY(IO_3)_4$ crystal structure.

Atom	Atom	Distance	Atom	Atom	Distance	Atom	Atom	Distance	Atom	Atom	Distance
Ag1	$O53^{I}$	2.344(7)	Ag2	$O32^{II}$	2.379(6)	Y1	$O32^{II}$	2.279(6)	Y2	$O82^{IV}$	2.286(6)
Ag1	$O43^{II}$	2.478(5)	Ag2	O53	2.451(7)	Y1	$O33^{I}$	2.315(6)	Y2	$O83^{III}$	2.318(6)
Ag1	$O42^{II}$	2.537(6)	Ag2	$O41^{III}$	2.481(6)	Y1	O11	2.355(6)	Y2	O81	2.355(6)
Ag1	O41	2.556(6)	Ag2	$O33^{II}$	2.689(6)	Y1	$O42^{II}$	2.380(6)	Y2	O61	2.356(6)
Ag1	O81	2.574(6)	Ag2	O52	2.689(6)	Y1	O21	2.395(7)	Y2	O71	2.377(6)
Ag1	O51	2.758(6)	Ag2	$O11^{III}$	2.694(6)	Y1	$O13^{II}$	2.400(6)	Y2	O43	2.392(5)
Ag1	$O52^{V}$	2.822(6)	Ag2	$O42^{III}$	2.789(6)	Y1	O41	2.415(6)	Y2	$O63^{IV}$	2.458(6)
Ag1	O82	3.070(6)	Ag2	O31	2.875(6)	Y1	O31	2.423(6)	Y2	O51	2.502(6)
I1	O11	1.824(6)	I2	O21	1.832(7)	I3	O31	1.817(6)	I4	O41	1.827(6)
I1	O12	1.809(6)	I2	O22	1.798(6)	I3	O32	1.810(6)	I4	O42	1.817(5)
I1	O13	1.803(6)	I2	O23	1.797(7)	I3	O33	1.797(5)	I4	O43	1.817(5)
I5	O51	1.804(7)	I6	O61	1.815(6)	I7	O71	1.825(6)	I8	O81	1.835(6)
I5	O52	1.787(6)	I6	O62	1.814(7)	I7	O72	1.798(6)	I8	O82	1.798(6)
I5	O53	1.800(7)	I6	O63	1.812(6)	I7	O73	1.806(7)	I8	O83	1.826(6)

Symmetry codes: ^{I} (x, 1-y, z+1/2) ; ^{II} (x, y-1, z) ; ^{III} (x, 1-y, z-1/2) ; ^{IV} (x, y+1, z) ; ^{V} (x, -y, z+1/2).

Table 2 Limit interatomic distances (Å) (with e.s.d) and limit bond angles (°) (with e.s.d) in $NaY(IO_3)_4$, $NaNd(IO_3)_4$, $NaGd(IO_3)_4$, $AgY(IO_3)_4$, $AgLa(IO_3)_4$, $AgNd(IO_3)_4$, $AgEu(IO_3)_4$, $AgGd(IO_3)_4$ and $AgBi(IO_3)_4$.

Bond lengths		Bond angles	
single crystal data			
Ag-O	2.344(7) – 3.070(6)	O-Ag-O	55.4(2) – 171.2(2)
Y-O	2.279(6) – 2.502(6)	O-Y-O	66.7(2) – 159.2(2)
I-O	1.787(6) – 1.835(7)		
Na-O	2.30(2) – 3.10(2)	O-Na-O	54.4(4) – 170.6(5)
Y-O	2.28(1) – 2.56(1)	O-Y-O	66.5(3) – 159.5(4)
I-O	1.78(1) – 1.84(1)		
Ag-O	2.372(8) – 3.185(9)	O-Ag-O	54.5(2) – 169.7(2)
La-O	2.411(7) – 2.664(7)	O-La-O	66.1(2) – 158.2(3)
I-O	1.790(7) – 1.837(7)		
Ag-O	2.352(5) – 3.095(4)	O-Ag-O	55.4(1) – 170.5(1)
Gd-O	2.316(4) – 2.539(4)	O-Gd-O	66.5(1) – 159.2(1)
I-O	1.793(4) – 1.831(4)		
Ag-O	2.35(1) – 3.176(9)	O-Ag-O	55.1(2) – 170.0(2)
Bi-O	2.325(9) – 2.592(9)	O-Bi-O	65.7(3) – 159.3(3)
I-O	1.780(9) – 1.836(9)		
powder data			
Na-O	1.94(6) – 3.21(5)	O-Na-O	53.2(2) – 170.2(2)
Nd-O	2.20(1) – 2.82(1)	O-Nd-O	62.5(2) – 159.1(6)
Na-O	2.18(6) – 3.19(7)	O-Na-O	54.4(2) – 166.6(2)
Gd-O	2.15(1) – 2.80(1)	O-Gd-O	63.0(4) – 161.7(4)
Ag-O	2.22(1) – 3.05(1)	O-Ag-O	54.0(3) – 174.9(3)
Nd-O	2.21(1) – 2.59(1)	O-Nd-O	63.6(3) – 162.8(3)
Ag-O	2.33(2) – 3.08(2)	O-Ag-O	55.3(5) – 174.5(6)
Eu-O	2.23(2) – 2.55(2)	O-Eu-O	64.6(6) – 158.9(6)

Table 3 Room-temperature dependence of the $^4F_{3/2}$ fluorescence decay time (τ) *versus* the *x* molar fraction of Nd^{3+} in $AgGd_{1-x}Nd_x(IO_3)_4$ and $AgLa_{1-x}Nd_x(IO_3)_4$ upon photoexcitation at 750 or 805 nm, respectively; and room-temperature dependence of the $^2F_{5/2}$ fluorescence decay time (τ) *versus* *x* molar fraction of Yb^{3+} in $AgGd_{1-x}Yb_x(IO_3)_4$ upon irradiation at 980 nm.

x molar fraction in $AgGd_{1-x}Nd_x(IO_3)_4$	τ (ms)	x molar fraction in $AgLa_{1-x}Nd_x(IO_3)_4$	τ (ms)	x molar fraction in $AgGd_{1-x}Yb_x(IO_3)_4$	τ (ms)
0.02	0.145	0.02	0.156	0.02	0.566
0.05	0.137	0.05	0.135	0.05	0.545
0.09	0.120	0.09	0.119	0.09	0.535
0.17	0.100	0.15	0.097	0.17	0.490

Table 4 Crystal data and structure refinement details for $NaY(IO_3)_4$, $AgY(IO_3)_4$, $AgLa(IO_3)_4$, $AgGd(IO_3)_4$ and $AgBi(IO_3)_4$.

Formula	$NaY(IO_3)_4$	$AgY(IO_3)_4$	$AgLa(IO_3)_4$	$AgGd(IO_3)_4$	$AgBi(IO_3)_4$
M ($g.mol^{-1}$)	811.5	896.38	946.38	964.72	1016.45
Crystal system	monoclinic	monoclinic	monoclinic	monoclinic	monoclinic
Space group	*Cc*	*Cc*	*Cc*	*Cc*	*Cc*
a (Å)	31.159(3)	31.277(3)	31.931(3)	31.374(3)	31.606(3)
b (Å)	5.553(1)	5.547(1)	5.696(1)	5.581(1)	5.588(1)
c (Å)	12.537(2)	12.556(2)	12.995(2)	12.638(2)	12.729(2)
β (°)	91.12(2)	91.11(2)	90.74(1)	91.13(1)	90.79(2)
V ($Å^3$)	2168.8(6)	2178.0(6)	2363.3(6)	2212.5(6)	2247.9(6)
Z	8	8	8	8	8
D_x ($g.cm^{-3}$)	4.97	5.47	5.32	5.79	6.01
μ (mm^{-1})	9.014	9.876	8.320	10.055	15.335
Crystal dim. (mm^3)	0.13×0.12×0.04	0.28×0.16×0.08	0.07×0.08×0.12	0.53×0.12×0.1	0.3×0.14×0.14
F(000)	2864	3152	3296	3352	3504
$N(hkl)_{collected}$	22414	24627	24340	38923	20581
$N(hkl)_{unique}$	4968	4958	5375	4984	5138
Contribution of inverted component	0.53(2)	0.56(1)	0.63(3)	0.53(1)	0.543(5)
Refined parameters	281	326	327	327	326
R_{int}	0.079	0.052	0.069	0.026	0.048
R_1 [(a)]	0.052	0.029	0.026	0.016	0.030
ωR_2 [(b)]	0.072	0.045	0.059	0.028	0.059
Goodness of fit S	1.073	1.073	1.067	1.112	1.059
$\Delta\rho_{max}/\Delta\rho_{min}$ ($e.Å^{-3}$)	1.294 and -1.403	1.034 and -1.278	1.095/-1.864	0.765 and -0.932	1.47 and -1.46

[(a)] $R_1 = \Sigma \, ||Fo|-|Fc||/\Sigma|Fo|$, [(b)] $\omega R_2 = [\Sigma(\omega(Fo^2-Fc^2)^2)/\Sigma(\omega(Fo^2)^2]^{1/2}$ with $\omega = 1/[(\sigma^2Fo^2)+(aP)^2+bP]$ and $P = (\max(Fo^2)+2Fc^2)/3$

Table 5 Crystal data and powder structure refinement details for $NaNd(IO_3)_4$, $NaGd(IO_3)_4$, $AgNd(IO_3)_4$ and $AgEu(IO_3)_4$.

Formula	$NaNd(IO_3)_4$	$NaGd(IO_3)_4$	$AgNd(IO_3)_4$	$AgEu(IO_3)_4$
M ($g.mol^{-1}$)	866.83	879.84	951.71	959.43
Crystal system	monoclinic	monoclinic	monoclinic	monoclinic
Space group	*Cc*	*Cc*	*Cc*	*Cc*
a (Å)	31.524(2)	31.335(2)	31.632(2)	31.491(2)
b (Å)	5.642(1)	5.596(1)	5.633(1)	5.600(1)
c (Å)	12.772(1)	12.642(1)	12.800(1)	12.695(1)
β (°)	90.88(1)	91.03(1)	90.93(1)	91.04(1)
V ($Å^3$)	2271.0(2)	2216.4(2)	2280.5(3)	2238.3(2)
Z	8	8	8	8
2θ range (°)	10.0 to 100.0	15.0 to 65.11	16.0 to 90.20	16.0 to 90.20
no. of parameters	114	162	78	77
R_{wp}	26.9	16.9	10.1	9.63
R_p	28.7	15.9	12.5	11.0
R_{exp}	25.44	7.84	7.93	7.08
χ^2	1.12	4.62	1.63	1.85
R_{Bragg}	6.46	8.51	4.57	4.46
no. of reflections	1187	401	955	937

Figure caption

Fig. 1 Representation of the $AgY(IO_3)_4$ crystal packing projected along the [010] direction. Silver and yttrium atoms are in the centre of blue and grey polyhedra, respectively. Iodine and oxygen atoms are represented by green and red circles, respectively.

Fig. 2 Transmittance curves of $NaY(IO_3)_4$ (•••), $NaGd(IO_3)_4$ (**---**), $AgY(IO_3)_4$ (---), $AgLa(IO_3)_4$ (···), $AgGd(IO_3)_4$ (—) and $AgBi(IO_3)_4$ (—) in the 2.5 to 16 μm region (grey bands correspond to the atmospheric transparency windows II and III).

Fig. 3 Room-temperature emission spectra of $AgGd_{0.98}Nd_{0.02}(IO_3)_4$ obtained upon photoexcitation of the $^4F_{3/2}$ excited multiplet state of the neodymium ion at 750 nm.

Fig. 4 Concentration dependence of Nd^{3+} decay time in the $AgGd(IO_3)_4$, $AgLa(IO_3)_4$ hosts compared to α-$Y(IO_3)_3$ and β-$Y(IO_3)_3$ hosts[36] at room-temperature.

Fig. 5 Room-temperature emission spectra of $AgGd_{0.98}Yb_{0.02}(IO_3)_4$ obtained upon irradiation of the $^4F_{5/2}$ excited multiplet state of the neodymium ion at 980 nm.

Fig. 6 Concentration dependence of Yb^{3+} decay time in the $AgGd(IO_3)_4$ host compare to α-$Y(IO_3)_3$ and β-$Y(IO_3)_3$ hosts[36] at room-temperature.

Fig. 7 Observed (points), calculated (line) and difference (bottom line) X-ray diffraction pattern of $AgEu(IO_3)_4$ measured on D8 Bruker (λ = 1.54056 Å). Vertical lines indicate Bragg positions of the contribution phase $AgEu(IO_3)_4$.

Table caption

Table 1 Selected interatomic distances (Å) (with e.s.d) in $AgY(IO_3)_4$ crystal structure.

Table 2 Limit interatomic distances (Å) (with e.s.d) and limit bond angles (°) (with e.s.d) in $NaY(IO_3)_4$, $NaNd(IO_3)_4$, $NaGd(IO_3)_4$, $AgY(IO_3)_4$, $AgLa(IO_3)_4$, $AgNd(IO_3)_4$, $AgEu(IO_3)_4$, $AgGd(IO_3)_4$ and $AgBi(IO_3)_4$.

Table 3 Room-temperature dependence of the $^4F_{3/2}$ fluorescence decay time (τ) *versus* the *x* molar fraction of Nd^{3+} in $AgGd_{1-x}Nd_x(IO_3)_4$ and $AgLa_{1-x}Nd_x(IO_3)_4$ upon photoexcitation at 750 or 805 nm, respectively; and room-temperature dependence of the $^2F_{5/2}$ fluorescence decay time (τ) *versus* *x* molar fraction of Yb^{3+} in $AgGd_{1-x}Yb_x(IO_3)_4$ upon irradiation at 980 nm.

Table 4 Crystal data and structure refinement details for $NaY(IO_3)_4$, $AgY(IO_3)_4$, $AgLa(IO_3)_4$, $AgGd(IO_3)_4$ and $AgBi(IO_3)_4$.

Table 5 Crystal data and powder structure refinement details for $NaNd(IO_3)_4$, $NaGd(IO_3)_4$, $AgNd(IO_3)_4$ and $AgEu(IO_3)_4$.